Applied Nanoscience (2018) 8:557–565
https://doi.org/10.1007/s13204-018-0677-0

ORIGINAL ARTICLE

Enlargement of photocatalytic efficiency of $BaSnO_3$ by indium doping for thiophene degradation

Tariq R. Sobahi[1] · M. S. Amin[2,3] · R. M. Mohamed[1,4]

Received: 6 November 2017 / Accepted: 6 February 2018 / Published online: 24 February 2018

Abstract

$BaSnO_3$ nanorods were produced by a sol–gel mode. Indium, as dopant, was introduced to the surface of $BaSnO_3$ via photo-assisted deposition technique. Phase composition, microstructure and surface area of the synthesized samples were identified via X-ray diffraction, field emission scanning electron microscopy (FESEM) and BET techniques, respectively. State of element, band gap energy and position of emission energy were measured via X-ray photoelectron spectroscopy (XPS), ultraviolet and visible spectroscopy (UV–Vis) and photoluminescence emission spectra (Pl), respectively. Furthermore, the catalytic performance of both $BaSnO_3$ and In/$BaSnO_3$ specimens was implemented for photocatalytic destruction of thiophene solution via visible light irradiation. XPS results displayed the patterns corresponding to the In–In at about 443.8 eV, illustrating the presence of indium metal in a nano-sized scale. A red shift was observed after indium loading within the $BaSnO_3$ lattice which was proved via the UV–Vis analysis. 100% oxidation efficiency percent was attained using 0.3 wt% In/$BaSnO_3$ photocatalyst after 1 h reaction time. The enhancement of the photocatalytic activity was mainly attributed to the indium doping into $BaSnO_3$ as a result of its capability to hinder the e^-–h^+ re-combination. The catalyst was reused up to five cycles without any change in its efficiency.

Keywords In doping · $BaSnO_3$ · Photocatalyst · Thiophene oxidation

Introduction

Sulfur elimination from fluidized catalytic cracker naphtha to the desirable restriction is a crucial issue in the refining industry. One of the major components in gasoline pool is The FCC naphtha. Thiophenes are considered the preeminent sulfur-incorporating compounds in FCC naphtha. Thiophenes are inert relative to other sulfur-containing compounds since they are aromatic. Hydrodesulfurization process is one of the most important methods that have been utilized in removal of thiophenes (Teng-fei et al. 2015; Boukoberine and Hamada 2016; Kabe et al. 1992; Gates and Topsoe 1997; Ma et al. 1994, 1995; Olguin-Orozco et al. 1997; Kilanowski et al. 1978). The drawbacks of this method are its high cost besides, affecting the octane number of gasoline. Many alternative efficient and economical methods have been examined, for thiophene elimination, to overcome these drawbacks such as pervaporation method (Lin et al. 2009; Bettermann and Staudt 2009; Qi et al. 2006; Jain et al. 2015, 2016). The superiority of pervaporation method is the relatively lower demands of temperature and pressure compared to those in hydrodesulfurization method and it was concluded that thiophene could be removed successfully from FCC gasoline up to any desirable limit via the pervaporation method. Other successful alternative techniques were investigated too for thiophene elimination. For instance, reactive adsorption using solid adsorbents and H_2 (Song 2003), selective adsorption in absence of H_2 at

✉ Tariq R. Sobahi
tsohabi@gmail.com

M. S. Amin
mohamedsamin@hotmail.com

R. M. Mohamed
redama123@yahoo.com

[1] Department of Chemistry, Faculty of Science, King Abdulaziz University, PO Box 80203, Jeddah 21589, Saudi Arabia

[2] Department of Chemistry, Science College, Taibah University, Medina, Saudi Arabia

[3] Chemistry Department, Faculty of Science, Ain Shams University, Cairo, Egypt

[4] Advanced Materials Department, Central Metallurgical R&D Institute, CMRDI, P.O. Box 87, Helwan, Cairo, Egypt

ambient temperature (Ma et al. 2001, 2002a, b; Velu et al. 2002; 2003a, b; Qi et al. 2015), hydrodesulfurization accompanied with distillation (Rock 2002; Rock and Shorey 2003), absorption using ionic liquids (Bösmann et al. 2001; Zhang and Zhang 2002; Mafi et al. 2016). Although there are broad scale applications of these processes they are very costly. Recently, different polymeric materials such as polyhedral oligomeric silsesquioxane (POSS), polyvinylidene fluoride (PVDF), polyimide (PI), polyethylene glycol (PEG), etc. were handled as membranes for thiophene withdrawal from gasoline (Yu et al. 2015; Konietzny et al. 2014; Amaral et al. 2014; Qu et al. 2010; Chen et al. 2008; Zhao et al. 2008; Jain et al. 2017; Yang et al. 2014; Liu et al. 2014a, b; Lin et al. 2012, 2014; Yang et al. 2013). In modern trends, extraction desulfurization has been devoted to be the most effective and suitable method as a result of its mild operational conditions of temperature and pressure without any hydrogen consumption (Mokhtarani et al. 2014). Recently, there has been an extensive significance in heterogeneous photocatalysis adopting semiconductors for the pollutant removal. The main advantage of photocatalysis is that it provides a more environmentally sustainable solution for pollutant removal without any need for further treatment. Thiophene destruction over polyaniline/mesoporous Cu_2O nanocomposites was investigated (Mohamed and Aazam 2014). It was found that the semiconductor/conductive polymer composite had large photocatalytic activity under visible light. TiO_2 was doped with Ag and the resulted photocatalyst was supported on MWCNTs, and then Ag–TiO_2/MWCNT photocatalysts were used to degrade thiophene by photocatalysis under visible light irradiation in an aqueous solution and it was found that 0.02:1.0:0.05 was the optimum mass ratio of MWCNT:TiO_2:Ag, which lead to about 100% photocatalyst's experimental performance for thiophene oxidation in a 600 mg/l solution within 30 min (Aazam 2014). Other researchers studied the photooxidation of thiophene using different materials as, RuO_2/SO_2–TiO_2 (Lina et al. 2016), NiO/$AgInS_2$ nanoparticles (Baeissa 2014), Pd/ZrO_2–chitosan nanocomposite (Abdelaala and Mohamed 2014), Ag–$BiVO_4$ (Gao et al. 2013), TiO_2/Cr-MCM-41 (Marques et al. 2008), TiO_2 (Dedual et al. 2014), TiO_2/Ni-ZSM-5 (Wang et al. 2013). Pt/PbS nanoparticles (Mohamed and Aazam 2014), MoO_3/γ-Al_2O_3 (Xue et al. 2017), titania/MWCNT composite (Barmala et al. 2015). The notable and wonderful characteristics involving dielectric, electrical and optical properties of Barium stannate (Zhang et al. 2007; Mizoguchi et al. 2004), makes it one of the most significant materials to be used as photocatalyst, catalyst support, solar cell and capacitor, etc. (Wang et al. 2014; Shin et al. 2013; Cerda et al. 2002). A new simple coprecipitation method was applied to prepare nanocrystalline barium stannate (Moshtaghi et al. 2016). Many other attempts had been made to prepare barium stannate (Upadhyay et al. 1997; Reddy et al. 2001; Upadhyay 2013; Ihlefeld et al. 2008). Doped barium stannate could be prepared via different methods (Ansaree and Upadhyay 2015; Bévillon et al. 2008; Kumar et al. 2007; Singh et al. 2005; Wang et al. 2007). Indium is elected to be the dopant for different metal oxide nanostructures; this selection is attributed to its ability to magnify the photocatalytic activity properties of these metal oxides. Different morphologies of indium-doped ZnO nanostructures have been prepared via solvothermal method (Rezapourn and Talebian 2014). Indium-doped titania particles in a nano-scale were prepared via a sol–gel method (Tahir and Amin 2015). In addition, indium doping of different materials were prepared by various methods (Singh et al. 2010; Chava and Kang 2017; Feng et al. 2016; Kumar et al. 1999; Nishio et al. 2006; Saquib et al. 2008; Yang et al. 2018). In this project, we address the preparation of a novel In/$BaSnO_3$ nanocomposite through sol–gel method and we apply this material for thiophene degradation.

Experimental techniques

Synthesis of $BaSnO_3$

Chemicals in this study were used without further purification as they are of analytical grade. 1 mmol of tin(IV) isopropoxide solution and 1 mmol of barium nitrate were dissolved in a mixture containing 30 ml of ethanol, 20 ml of de-ionized water and 0.05 mmol of HNO_3. The resultant mixture was stirred for 90 min, then added to glass vessel and kept in a microwave at 180 °C for 20 min. After that, the product was gathered via centrifugation and then washed many times using absolute ethanol and de-ionized water. The delivered sample was left to dry at about 80 °C overnight and air-heated at 400 °C for 1 h. The produced specimen was titled $BaSnO_3$.

Synthesis of In/$BaSnO_3$

The synthesized $BaSnO_3$ nanorods were added to 20 ml of distilled water containing suitable amount of indium(III) nitrate hydrate. The suspension was stirred and irradiated overnight by strong UV lamp. The resultant material was gathered and heated at 140 °C for 1 h in air. In was permitted to be doped within $BaSnO_3$ structure with the ratios of 0.1, 0.2, 0.3, and 0.4% wt, and the products were named 0.1 wt% In/$BaSnO_3$, 0.2 wt% In/$BaSnO_3$, 0.3 wt% In/$BaSnO_3$ and 0.4 wt% In/$BaSnO_3$, respectively.

Identification techniques

X-ray diffracto-grams of both $BaSnO_3$ and In–$BaSnO_3$ nanocomposites were measured using X-ray diffraction (XRD)

analysis via Cu-Kα radiation ($\lambda = 1.540$ Å). A Nova-2000 instrument was adopted for specific surface area determination of the synthesized $BaSnO_3$ and In–$BaSnO_3$ nanocomposites through N_2-adsorption at 77 K. Before each measurement, specimens were heated at about 250 °C for 4 h to remove gases from these specimens. Band gap energies corresponding to the synthesized $BaSnO_3$ as well as In–$BaSnO_3$ nanocomposites were measured applying a spectro-photometer (V-570, JASCO, Japan) via determination of UV–Visible diffuse reflectance spectra (UV–Vis-DRS) in air at ambient temperature within the wavelength range of 200 up to 800 nm. Morphology and microstructure of the prepared nanocomposites were investigated using scanning electron microscopy (JEOL-JEM-5410). The elemental analysis of the synthesized specimens was attained using X-ray photoelectron spectroscope (XPS) of Thermo Scientific K-ALPHA type, England.

Photocatalytic efficiency

A pyrex reaction cell was handled for thiophene oxidation using the photocatalyst through O_2, the oxidant, bubbling in a steady-state flow. 1 g/l photocatalyst was spread in thiophene-containing acetonitrile solution (initial content of sulfur = 6×10^2 ppm). After that, the suspension was agitated in the absence of light for 0.5 h, to attain equilibrium, before being irradiated by a 125-W mercury lamp with a UV cut filter. The reaction solution temperature was then kept at low temperature (12 °C) through cooling water flow. At the end of the reaction and after catalyst separation, the major and minor products were analyzed by GC-FPD (Agilent 7890, FFAP column) and GC–MS.

Results and discussion

Phase composition, morphology and microstructure

XRD diffractograms of both $BaSnO_3$ and In/$BaSnO_3$ nanocomposites are illustrated in Fig. 1. The patterns of Fig. 1 indicate that $BaSnO_3$ and In/$BaSnO_3$ nanocomposites are primarily composed of $BaSnO_3$ phase (JCPDS Card: 15-0780), this result reveals that the $BaSnO_3$ skeleton will persist after indium doping. It is clear from the diffraction pattern of In/$BaSnO_3$ sample that the peak characteristic to indium are absent. The absence of the characteristic peaks of indium in the patterns of In/$BaSnO_3$ sample may be ascribed to the low indium-dopant content. Evidently, the data illustrate that indium is well dispersed within the $BaSnO_3$ lattice. In fact, indium played a prominent aspect in the process of crystallization since the characteristic diffraction peaks of

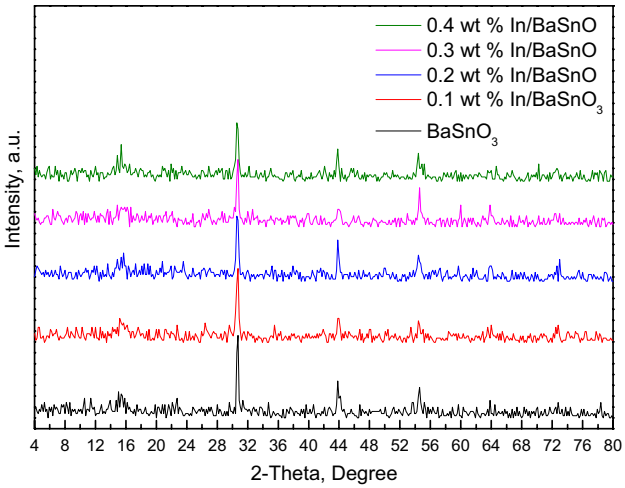

Fig. 1 XRD patterns of $BaSnO_3$ and In/$BaSnO_3$ nanocomposites

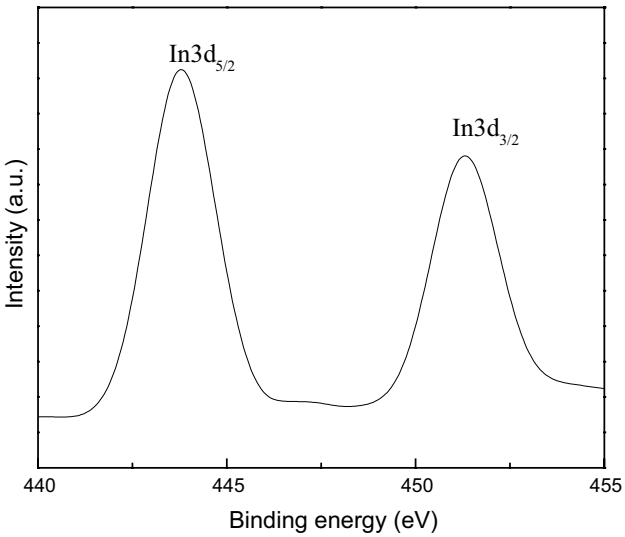

Fig. 2 XPS spectra of In3d for the 0.3 wt% In/$BaSnO_3$ nanocomposite

$BaSnO_3$ phase became broader and the diffraction peaks' intensities became lesser by increasing indium loading.

XPS spectra of In3d for the 0.3 wt% In/$BaSnO_3$ nanocomposite are displayed in Fig. 2. The existence of the peaks committed to the indium–indium at about 443.8 and 451.3 eV for $In3d_{5/2}$ and $In3d_{3/2}$, respectively, confirms the formation of indium metal in a nano-sized scale.

The SEM micrographs of $BaSnO_3$ and In/$BaSnO_3$ nanocomposites are presented in Fig. 3. The results reveal that as weight percent of indium metal increases, the dispersion on the surface of $BaSnO_3$ nanorods increases and this finding is valid up to 0.3 wt% of indium dopant (Fig. 3a–d). On the contrary, indium is doped as aggregate by increasing weight percent of indium over 0.3 wt% as shown in Fig. 3e.

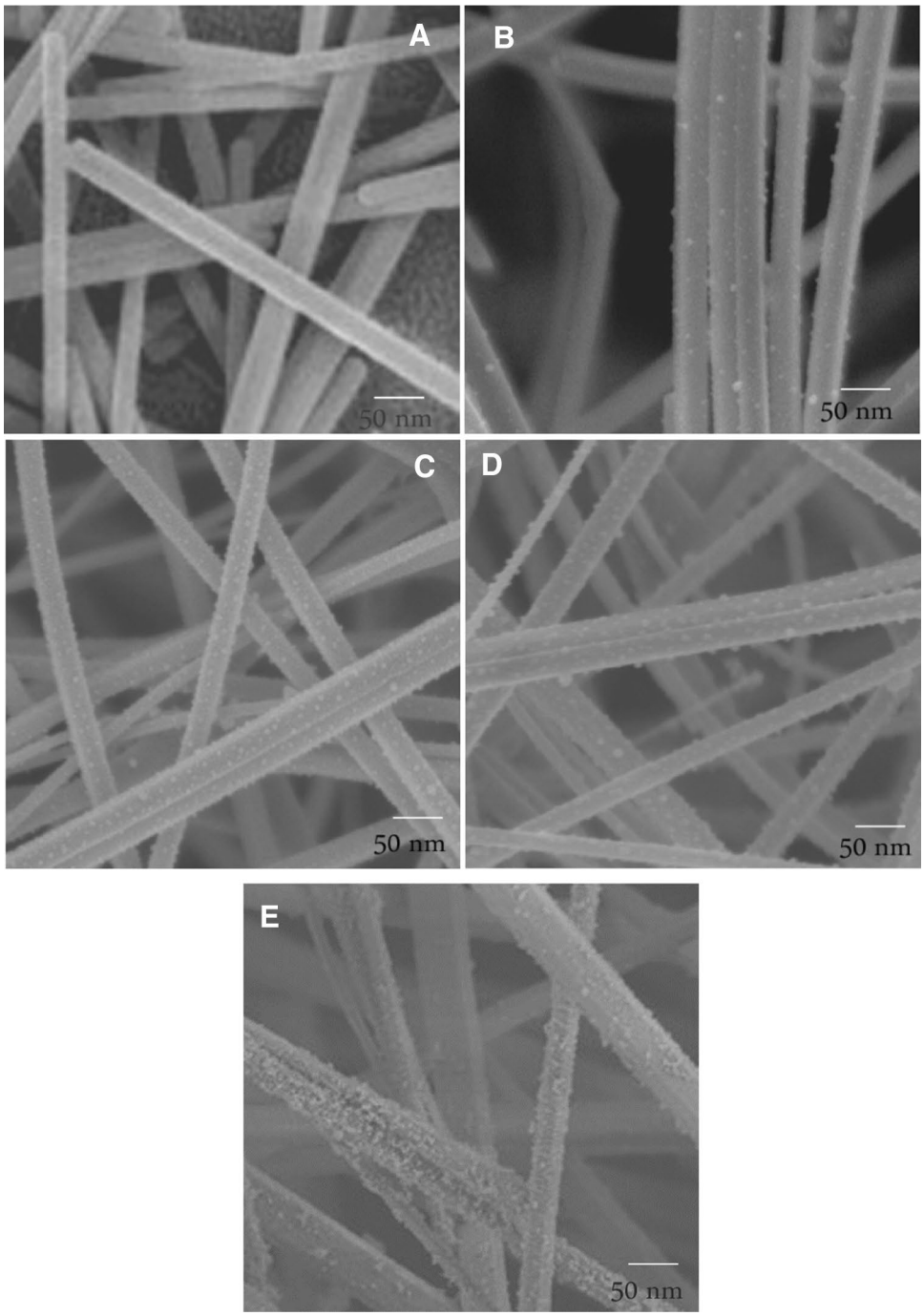

Fig. 3 SEM images of $BaSnO_3$ and In/$BaSnO_3$ nanocomposites, where wt% of In is 0.0 (**a**); 0.1 (**b**); 0.2 (**c**); 0.3 (**d**); and 0.4 (**e**)

Surface area measurement

Specific surface areas (S_{BET}) of both $BaSnO_3$ and In/$BaSnO_3$ nanocomposites were determined. The surface area of the parent $BaSnO_3$ and In/$BaSnO_3$ nanocomposites are given in Table 1. The S_{BET} values are found to be 45, 43, 41, 39 and 34 m^2/g for $BaSnO_3$, 0.1 wt% In/$BaSnO_3$, 0.2 wt% In/$BaSnO_3$, 0.3 wt% In/$BaSnO_3$ and 0.4 wt% In/$BaSnO_3$, respectively. In fact, the bigger characters of the specific surface area of $BaSnO_3$ in comparison to those of

Table 1 BET surface area of $BaSnO_3$ and In/$BaSnO_3$ nanocomposites

Sample	Surface area (m^2/g)
$BaSnO_3$	45
0.1 wt% In/$BaSnO_3$	43
0.2 wt% In/$BaSnO_3$	41
0.3 wt% In/$BaSnO_3$	39
0.4 wt% In/$BaSnO_3$	34

the In/$BaSnO_3$ samples reveal that indium doping causes some pores to be blocked.

Optical characterization

The spectra corresponding to UV–Vis diffuse reflectance of $BaSnO_3$ as well as In/$BaSnO_3$ nano-materials are demonstrated in Fig. 4. The results of Fig. 4 illustrates that the introduction of indium metal into the $BaSnO_3$ lattice causes a shift of spectra towards higher wavelengths from 526 to 653 nm (red shift) by the various percentages of indium metal, comparing to $BaSnO_3$wavelength at nearly 400 nm. The band gaps for both $BaSnO_3$ and In/$BaSnO_3$ nanocomposites were determined from their own spectra of reflection found in the form proposed by Kumar et al. (1999), the band gap characters of the both synthesized nanocomposites are given in Table 2. Evidently, it is obvious from the data of Table 2 that the band gap energy decreases with increasing the weight percentages of the dopant indium. The values of band gap were found to be 3.1, 2.36, 2.16, 1.92 and 1.90 eV for the parent $BaSnO_3$, 0.1 wt% In/$BaSnO_3$, 0.2 wt% In/$BaSnO_3$, 0.3 wt% In/$BaSnO_3$ and 0.4 wt% In/$BaSnO_3$, respectively. This finding illustrates that indium doping enhances the photocatalytic activity of the catalyst via its band gap narrowing.

The deportation of holes and photogenerated electrons was studied via investigating photoluminescence (Pl) emission spectra. The PI emission spectra for the different investigated samples are shown in Fig. 5. It is obvious from the illustrations of Fig. 5 that the intensity of Pl is largely decreased with increasing the indium metal percentage. Moreover, separation of the photogenerated electron–hole couples occurs. This finding might be accredited to the capturing of photogenerated electrons from the CB by indium metal which acts as a trapping center. It is generally acknowledged that an enhancement in light retention of the catalysts in the wave length range of the visible region may occur as a result of the rare metal nanoparticles' embodiment into catalysts made of semiconductors. And so a deflection of the absorption threshold towards higher values of wavelengths occurs pointing out a reduction in the band gap energy. Consequently, extra photogenerated electrons along with holes will cooperate in the photocatalytic reaction. In the current study, indium implies to vary the interface of $BaSnO_3$ in such a manner that develops the system in which photo-originated charge carriers experience reconsolidation. And so, it will strengthen $BaSnO_3$ to be highly stimulated in the visible region. On the other hand, the displacement in the location of emission could be correlated to the conduction band (CB) of $BaSnO_3$ as a semiconductor and the charge transfer between the indium-generated bands.

Table 2 Band gap of $BaSnO_3$ and In/$BaSnO_3$ nanocomposites

Sample	Band gap energy (eV)
$BaSnO_3$	3.10
0.1 wt% In/$BaSnO_3$	2.36
0.2 wt% In/$BaSnO_3$	2.16
0.3 wt% In/$BaSnO_3$	1.92
0.4 wt% In/$BaSnO_3$	1.90

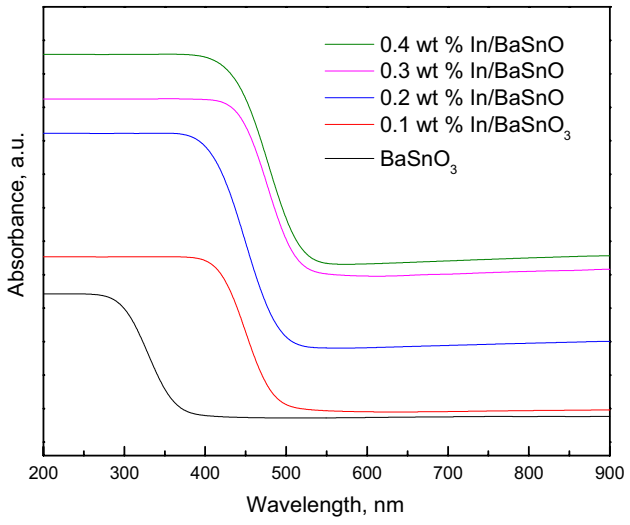

Fig. 4 UV–Vis absorption spectra of $BaSnO_3$ and In/$BaSnO_3$ nanocomposites

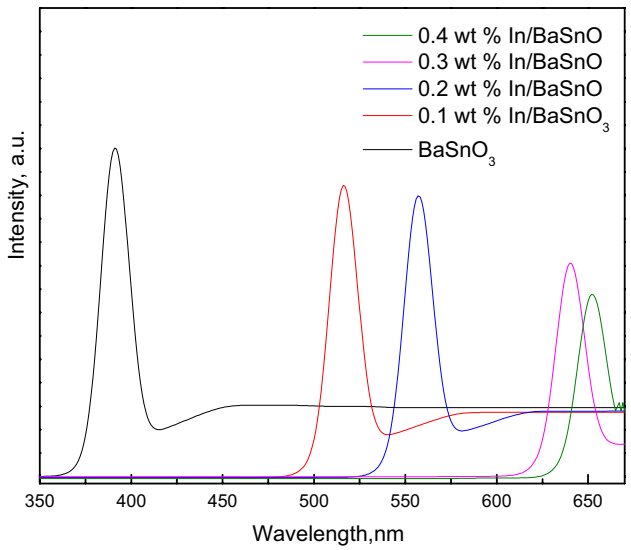

Fig. 5 Pl spectra of $BaSnO_3$ and In/$BaSnO_3$ nanocomposites

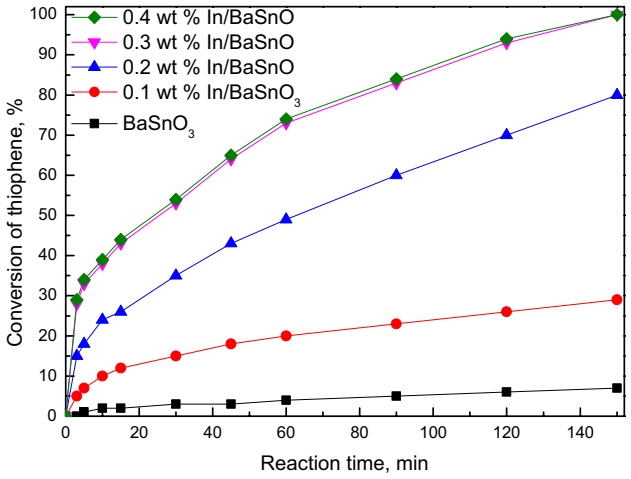

Fig. 6 Effect of catalyst type on photocatalytic conversion of thiophene

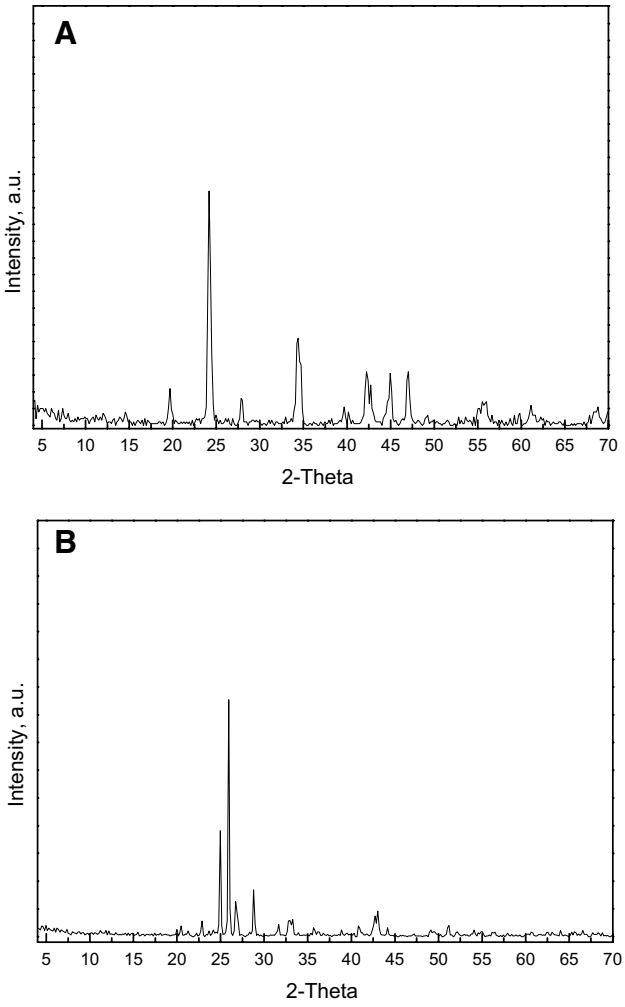

Fig. 7 **a** XRD pattern of the precipitate 1, **b** XRD pattern of the precipitate 2

Photocatalytic efficiency

Effect of catalyst kind

Figure 6 shows the photocatalytic degradation of thiophene compound over both $BaSnO_3$ and In/$BaSnO_3$ nanocomposites in the wavelength of the visible light. The examination was accomplished using the subsequent settings: 500 mL of thiophene solution having the concentration 600 ppm and 0.4 g/l catalyst. The results confirm the lower activity of $BaSnO_3$ photocatalyst beneath visible light. Moreover, the photocatalytic efficiency of In/$BaSnO_3$ doped with various loadings of In is increased in the following order: 0.1 wt% In/$BaSnO_3$ < 0.2 wt% In/$BaSnO_3$ < 0.3 wt% In/$BaSnO_3$ ≤ 0.4 wt% In/$BaSnO_3$, this finding is in agreement with those found in SEM, XRD, and band gap investigations.

Concerning the investigation of the photoproducts, the gas from the products' outlet is introduced to 0.2 M NaOH aqueous solution. When 0.2 M $Ba(NO_3)_2$ aqueous solution was added into the latter NaOH aqueous solution, a precipitate of white color was produced (designated as precipitate 1). The XRD pattern of precipitate 1 is illustrated in Fig. 7a. The XRD pattern proves the presence of $BaCO_3$, which is in acceptable convenience with the standard card of ICDD-PDF no. 05-0378. This finding ensures that thiophene can be oxidized to CO_2 in the presence of photocatalyst and captured in the NaOH aqueous solution. Meanwhile, if HNO_3 solution is added to precipitate 1, part of the white precipitate will still remain without dissolving in HNO_3 solution, designated as precipitate 2. The XRD diffractogram of precipitate 2 is displayed in Fig. 7b. The data of Fig. 7b indicate the formation of $BaSO_4$, which agrees with the standard card of ICDD-PDF no. 24-1035. This illustrates that the sulfur atom in thiophene can be oxidized to SO_3 in the presence of the photocatalyst. In conclusion, thiophene could be readily photocatalytically oxidized to both CO_2 and SO_3. And so, the photocatalytic degradation of thiophene will be as follows:

$$\text{Thiophene} + \text{photo-catalyst} \longrightarrow CO_2 + SO_3 + H_2O.$$

Effect of photocatalyst loading

The photocatalyst loading is considered another crucial factor that governs photocatalytic destruction of thiophene solution under Vis light irradiation. In this investigation, 0.3 wt% In/$BaSnO_3$ having loadings ranging from 0.2 up to 1.4 g/l in 600 mg/l thiophene solutions, were operated. The data of Fig. 8 illustrates that the time needed for thiophene oxidation decreases from 150 to 60 min by increasing the catalyst dose from 0.2 up to 0.8 g/l, respectively. On the contrary, further

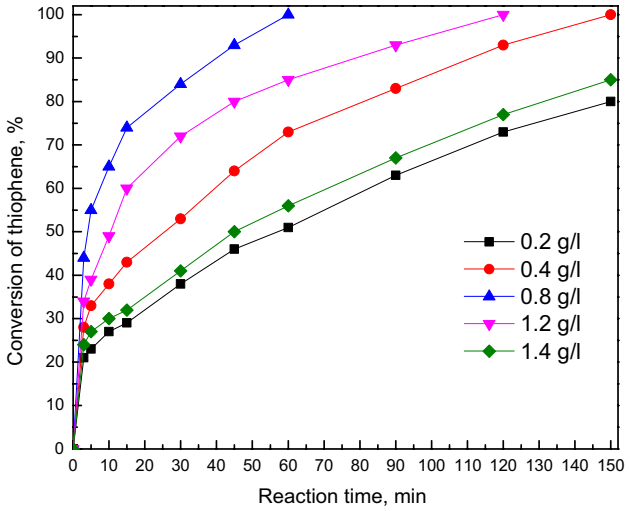

Fig. 8 Effect of loading of 0.3 wt% In/$BaSnO_3$ on photocatalytic conversion of thiophene

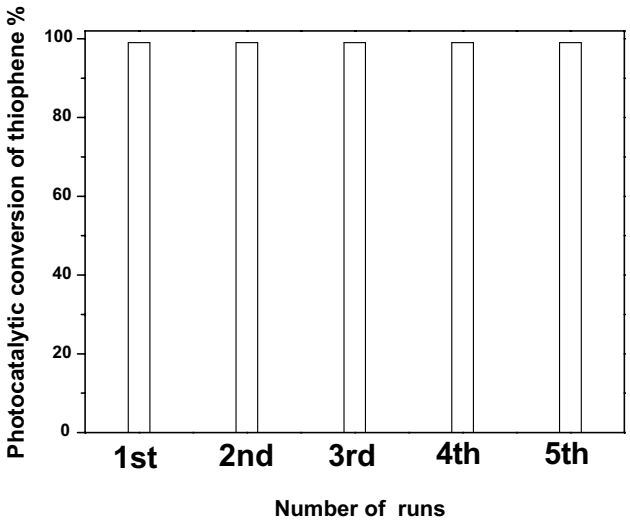

Fig. 9 Recycling and reusing of 0.3 wt% In/$BaSnO_3$ photocatalysts for photocatalytic conversion of thiophene

increase of the photocatalyst dose, above 0.8 g/l, leads to a repeated expansion in the reaction time up to 150 min. Actually, the increase of the photocatalyst dose will develop the total number of active centers on the photocatalyst (Nishio et al. 2006). And so, the number of the absorbed photons and thiophene molecules increases. However, at photocatalyst loadings above 0.8 g/l, the time needed to oxidize thiophene is increased due to the rendering of light entrance by the extra load of photocatalyst (Saquib et al. 2008).

Photocatalyst recovery

From the economic point of view, handling the photocatalyst several times is a serious subject. Photocatalytic activity of 0.3 wt% In/$BaSnO_3$ photocatalyst after recycling five times is shown in Fig. 9. The data confirm that the photocatalytic activity remains without change after recycling up to about five times. Hence, recycling and separation of 0.3 wt% In/$BaSnO_3$ photocatalyst could be preceded easily.

Conclusion

On the basis of our study, the subsequent conclusions could be stated

1. In/$BaSnO_3$, photocatalyst was profitably synthesized and verified to be a talented catalyst due to its great oxidation capability of pollutants in the wavelength range of visible light region.
2. Weight percentage of doped indium in $BaSnO_3$ controls the red shift phenomenon.
3. In/$BaSnO_3$ with a 0.3 wt% of In performed the greatest catalytic efficiency.
4. The synthesized photocatalyst is considered to be an efficient photocatalytic catalyst towards water disinfection.
5. Optimum conditions in our study were found to be; 0.3 wt% In/$BaSnO_3$, 0.8 g/l photocatalyst, 600 mg/l thiophene solution and these conditions yielded 100% oxidation of thiophene solution after 60 min of irradiation of visible light.
6. It was found that the photocatalyst under investigation remains impressive after about five cycles, which illustrates the talented recovery of the In/$BaSnO_3$ photocatalyst.

Acknowledgements This Project was funded by the Deanship of Scientific Research (DSR) at King Abdulaziz University, Jeddah, under Grant no. (G-71-130-38). The authors, therefore, acknowledge with thanks to DSR for technical and financial support.

References

Aazam ES (2014) Visible light photo catalytic degradation of thiophene using Ag–TiO_2/multi-walled carbon nano tubes nano composite. Ceram Int 40:6705–6711

Abdelaala MY, Mohamed RM (2014) Environmental remediation from thiophene solution by photocatalytic oxidation using a Pd/ZrO2–chitosan nanocomposite. Ceram Int 40:7693–7699

Amaral RA, Habert AC, Borges CP (2014) Activated carbon polyurethane membrane for a model fuel desulfurization by pervaporation. Mater Lett 137:468–470

Ansaree MJ, Upadhyay S (2015) Electrical characterization of porous La-doped $BaSnO_3$ using impedance spectroscopy. Ionics 21:2825–2838

Baeissa E (2014) Environmental remediation of thiophene solution by photocatalytic oxidation using $NiO/AgInS_2$ nanoparticles. J Ind Eng Chem 20:3270–3275

Barmala M, Moghadam AZ, Omidkhah MR (2015) Increased photocatalytic removal of sulfur using titania/MWCNT composite. Increased photo-catalytic removal of sulfur using titania/MWCNT composite. J Cent South Univ 22:1066–1070

Bettermann I, Staudt C (2009) Desulphurization of kerosene: pervaporation of benzothiophene/n-dodecane mixtures. J Membr Sci 343:119–127

Bévillon É, Geneste G, Chesnaud A, Wang Y, Dezanneau G (2008) Ab initio study of La-doped $BaSnO_3$ proton conductor. Ionics 14:293–301

Bösmann A, Datsevich L, Jess A, Lauter A, Schmitz C, Wasserscheid P (2001) Deep desulfurization of diesel fuel by extraction with ionic liquids. Chem Commun 23:2494–2495

Boukoberine Y, Hamada B (2016) Thiophene hydrodesulfurization over $CoMo/Al_2O_3$-CuY catalysts: Temperature effect study. Arab J Chem 9:522–527

Cerda J, Arbiol J, Dezanneau G, Dıaz R, Morante JR (2002) Perovskite-type $BaSnO_3$ powders for high temperature gas sensor applications. Sens Actuators 84:21–25

Chava RK, Kang M (2017) Improving the photovoltaic conversion efficiency of ZnO based dye sensitized solar cells by indium doping. J Alloys Compd 692:67–76

Chen J, Li J, Qi R, Ye H, Chen C (2008) Pervaporation performance of crosslinked polydimethyl siloxane membranes for deep desulfurization of FCC gasoline I. Effect of different sulfur species. J Membr Sci 322:113–121

Dedual G, MacDonald MJ, Alshareef A, Wub Z, Tsang DCW, Yip ACK (2014) Requirements for effective photocatalytic oxidative desulfurization of a thiophene-containing solution using TiO_2. J Environ Chem Eng 2:1947–1955

Feng CL, Duan JH, Liu G, Chen TC (2016) Effect of indium doping on ZnO: morphological change from nanorod to hexagonal nanodisk. Indian J Phys 90:347–352

Gao X, Fu F, Zhang L, Li W (2013) The preparation of $Ag–BiVO_4$ metal composite oxides and its application in efficient photocatalytic oxidative thiophene. Physica B 419:80–85

Gates BC, Topsoe H (1997) Reactivities in deep catalytic hydrodesulfurization: challenges, opportunities, and the importance of 4 methyldibenzothiophene and 4,6-dimethyl-dibenzothiophene. Polyhedron 16:3213–3217

Ihlefeld JF, Borland WJ, Maria J (2008) Synthesis and properties of barium titanate stannate thin films by chemical solution deposition. J Mater Sci 43:4264–4270

Jain M, Attarde D, Gupta S (2015) Removal of thiophene from n-heptane/thiophene mixtures by spiral wound pervaporation module: Modelling, validation and influence of operating conditions. J Membr Sci 490:328–345

Jain M, Attarde D, Gupta S (2016) Influence of hydrocarbon species on the removal of thiophene from FCC gasoline by using a spiral wound pervaporation module. J Membr Sci 507:43–54

Jain M, Attarde D, Gupta S (2017) Removal of thiophenes from FCC gasoline by using a hollow fiber pervaporation module: Modeling, validation, and influence of module dimensions and flow directions. Chem Eng J 308:632–648

Kabe T, Ishiharam A, Tajima H (1992) Hydrodesulfurization of sulfur containing polyaromatic compounds in light oil. Ind Eng Chem Res 31:1577

Kilanowski DR, Teeuwen H, De Beer VHJ, Gates BC, Schuit BCA, Kwart H (1978) Hydrodesulfurization of thiophene, benzothiophene, dibenzothiophene, and related compounds catalyzed by sulfided CoO– MoO3/-Al2O3: low-pressure reactivity studies. J Catal 55:129

Konietzny R, Koschine T, Rätzke K, Staudt C (2014) POSS-hybrid membranes for the removal of sulfur aromatics by pervaporation. Sep Purif Technol 123:175–182

Kumar V, Sharma SK, Sharma TP, Singh V (1999) Band gap determination in thick films from reflectance measurements. Opt Mater 12:115–119

Kumar A, Choudhary RNP, Singh BP (2007) Structural, dielectric and electrical properties of Te modified barium stannates using impedance analysis. J Mater Sci 42:8306–8310

Lin L, Zhang Y, Kong Y (2009) Recent advances in sulfur removal from gasoline by pervaporation. Fuel 88:1799–1809

Lin L, Wang A, Dong M, Zhang Y, He B, Li H (2012) Sulfur removal from fuel using zeolites/polyimide mixed matrix membrane adsorbents. J Hazard Mater 203:204–212

Lin L, Dong M, Liu C, Sun H, Zhang L, Zhang C, Deng P, Li Y (2014) Building movable bridges in membrane matrix by polyrotaxane crosslinking for sulfur removal. Mater Lett 126:59–62

Lina F, Jiangb Z, Tangb N, Zhangb C, Chenb Z, Liub T, Donga B (2016) Photocatalytic oxidation of thiophene on $RuO_2/SO_4^{2-}TiO_2$: Insights for cocatalyst and solid-acid. Appl Catal B 188:253–258

Liu K, Fang C-J, Li Z-Q, Young M (2014a) Separation of thiophene/n-heptane mixtures using PEBAX/PVDFcomposited membranes via pervaporation. J Membr Sci 451:24–31

Liu G, Zhou T, Liu W, Hu S, Pan F, Wu H, Jiang Z, Wang B, Yang J, Cao X (2014b) Enhanced desulfurization performance of PDMS membranes by incorporating silver decorated dopamine nanoparticles. J Mater Chem A 2:12907–12917

Ma X, Sakanishi K, Mochida I (1994) Hydrodesulfurization reactivities of various sulfur compounds in diesel fuel. Ind Eng Chem Res 33:218

Ma X, Sakanishi K, Isoda T, Mochida I (1995) Mochida, Hydrodesulfurization reactivities of narrow-cut fractions in a gas oil. Ind Eng Chem Res 34:748

Ma X, Sun L, Yin Z, Song C (2001) New approaches to deep desulfurization of diesel fuel, jet fuel, and gasoline by adsorption for ultra-clean fuels and for fuel cell applications. Am Chem Soc Div Fuel Chem Prepr 46:648

Ma X, Sun L, Song C (2002a) A new approach to deep desulfurization of gasoline, diesel fuel and jet fuel by selective adsorption for ultra-clean fuels and for fuel cell applications. Catal Today 77:107

Ma X, Sprague M, Sun L, Song C (2002b) Deep desulfurization of liquid hydrocarbons by selective adsorption for fuel cell applications. Am Chem Soc Div Petrol Chem Prepr 47:48

Mafi M, Mokhtarani B, Dehghani MR (2016) Removal of thiophene from model diesel oil with nitrate based ionic liquids at several temperatures. J Mol Liq 221:1104–1110

Marques FC, Canela MC, Stumbo AM (2008) Use of TiO_2/Cr-MCM-41 molecular sieve irradiated with visible light for the degradation of thiophene in the gas phase. Catal Today 133–135:594–599

Mizoguchi H, Eng HW, Woodward PM (2004) Woodward, Proping the electronic structures of ternary perovskite and pyrochlore oxides containing Sn^{4+} and Sb^{3+}. Inorg Chem 43:1667–1680

Mohamed RM, Aazam ES (2014a) Preparation and characterization of core–shell polyaniline/mesoporous Cu2O nanocomposites for the photo catalytic oxidation of thiophene. Appl Catal A 480:100–107

Mohamed RM, Aazam ES (2014b) New Visible-Light Pt/PbS Nanoparticle Photocatalysts for the Photocatalytic Oxidation of thiophene. Clean Soil Air Water 42:1–6

Mokhtarani B, Mansourzareh H, Mortaheb HR (2014) Phase behavior of nitrate based ionic liquids with thiophene and alkanes. Ind Eng Chem Res 53(3):1256–1261

Moshtaghi S, Zinatloo-Ajabshir S, Salavati-Niasari M (2016) Nanocrystalline barium stannate: facile morphology-controlled

preparation, characterization and investigation of optical and photocatalytic properties. J Mater Sci 27:834–842
Nishio J, Tokumura M, Znad HT, Kawase Y (2006) Photocatalytic decolorization of azo-dye with zinc oxide powder in an external UV light irradiation slurry photoreactor. J Hazard Mater 138:106–115
Olguin-Orozco E, Vrinat M, Cedeno L, Ramirez J, Boroque M, Lopez AA (1997) The use of TiO2–Al2O3 binary oxides as supports for Mo based catalysts in hydrodesulfurization of thiophene and dibenzothiophene. Appl Catal A 165:1–13
Qi R, Wang Y, Li J, Zhu S (2006) Sulfur removal from gasoline by pervaporation: the effect of hydrocarbon species. Sep Purif Technol 51:258–264
Qi H, Zhai S, Wang Z, Zhai B, An Q (2015) Designing recyclable Cu/ZrSBA-15 for efficient thiophene removal. Microporous Mesoporous Mater 217:21–29
Qu H, Kong Y, Lv H, Zhang Y, Yang J, Shi D (2010) Effect of crosslinking on sorption, diffusion and pervaporation of gasoline components in hydroxyl ethyl cellulose membranes. Chem Eng J 157:60–66
Reddy CVG, Manorama SV, Rao VJ (2001) Preparation and characterization of barium stannate: application as a liquefied petroleum gas sensor. J Mater Sci 12:137–142
Rezapourn M, Talebian N (2014) Synthesis and investigation of Indium doping and surfactant on themorphological, optical and UV/Vis photocatalytic properties of ZnO nanostructure. Ceram Int 40:3453–3460
Rock KL (2002) Ultra-low sulfur gasoline via catalytic distillation. In: Proceedings of the Fifth International Conference on Refinery Processing. AIChE 2002 spring national meeting, New Orleans, LA, 11–14 March, pp 200–205
Rock R, Shorey S (2003) Producing low sulfur gasoline reliably, AM-03 122. In: Proceedings of the NPRA 2003 annual meeting, San Antonio, TX, 23–25 March
Saquib M, Tariq MA, Haque MM, Muneer M (2008) Photocatalytic degradation of disperse blue 1 using UV/TiO_2/H_2O_2 process. J Environ Manag 88:300–306
Shin SS, Kim JS, Suk JH, Lee KD, Kim DW, Park JH, Cho IS, Hong KS, Kim JY (2013) Improved quantum efficiency of highly efficient perovskite BaSnO3-based dye-sensitized solar cells. ACS Nano 7:1027
Singh P, Parkash O, Kumar D (2005) DC conduction behaviour of niobium doped barium stannate. J Mater Sci 16:145–148
Singh G, Shrivastava SB, Jain D, Pandya S, Shripathi T, Ganesan V (2010) Effect of indium doping on zinc oxide films prepared by chemical spray pyrolysis technique. Bull Mater Sci 33:581–587
Song C (2003) An overview of new approaches to deep desulfurization for ultra-clean gasoline, diesel fuel and jet fuel. Catal Today 86:211–263
Tahir M, Amin NS (2015) Indium-doped TiO2 nanoparticles for photocatalytic CO2 reduction with H2O vapors to CH4. Appl Catal B 162:98–109
Teng-fei W, Ye Z, Hui G, Ming-xing T, Li-gong Z, Zhan-jun LÜ, Xue-kuan LI (2015) Hydrodesulfurization of thiophene over Mo/AC catalyst presulfided by ammonium thiosulfate. J Fuel Chem Technol 43:202–207
Upadhyay S (2013) High temperature impedance spectroscopy of barium stannate, BaSnO3. Bull Mater Sci 36:1019–1036
Upadhyay S, Parkash O, Kumar D (1997) Preparation and characterization of barium stannate $BaSnO_3$. J Mater Sci Lett 16:1330–1332
Velu S, Ma X, Song C (2002) Zeolite-based adsorbent for desulfurization of jet fuel by selective adsorption. Am Chem Soc Div Fuel Chem Prepr 47:447
Velu S, Ma X, Song C (2003a) Fuel cell grade gasoline production by selective adsorption for removing sulfur. Am Chem Soc Div Petrol Chem Prepr 48:58
Velu S, Watanable S, Ma X, Song C (2003b) Development of selective adsorbent for removing sulfur from gasoline for fuel cell applications. Am Chem Soc Div Petrol Chem Prepr 48:56
Wang S, Yang Z, Zhou G, Lu M, Zhou Y, Zhang H (2007) Combustion synthesis and luminescence characteristic of Eu^{3+}-doped barium stannate nanocrystals. J Mater Sci 42:6819–6823
Wang L, Cai H, Li S, Mominou N (2013) Mominou, Ultra-deep removal of thiophene compounds in diesel oil over catalyst TiO_2/Ni-ZSM-5 assisted by ultraviolet irradiating. Fuel 105:752–756
Wang W, Liang S, Ding K, Bi J, Yu JC, Keung Wong P, Wu L (2014) Microwave hydrothermal synthesis of $MSnO_3$ (M^{2+}, Ca^{2+}, Sr^{2+}, Ba^{2+}): effect of M^{2+} on crystal structure and photocatalytic properties. J Mater Sci 49:1893
Xue L, Zhang D, Xu Y, Liu X (2016) Adsorption of thiophene compounds on MoO_3/ϫ-Al_2O_3 catalysts with different mesopore sizes. Microporous Mesoporous Mater. https://doi.org/10.1016/j.micromeso.2016.03.004
Yang Z, Wang T, Zhan X, Li J, Chen J (2013) Poly [bis(p-methylphenyl) phosphazene] pervaporative membranes for separating organo sulfur compounds from n-heptane and its surface functionalization. Ind Eng Chem Res 52:13801–13809
Yang Z, Zhang W, Wang T, Li J (2014) Improved thiophene solution selectivity by Cu^{2+}, Pb^{2+} and Mn^{2+} ions inpervaporative poly [bis (p-methylphenyl) phosphazene] desulfurization membrane. J Membr Sci 454:463–469
Yang D, Huang Z, Wu S, Xiong K, Zhang X, Zheng B, Nadimicherla R, Fu R, Wu D (2018) Polymer 137:195–200
Yu S, Pan F, Yang S, Ding H, Jiang Z, Wang B, Li Z, Cao X (2015) Enhanced pervaporation performance of MIL-101(Cr) filled polysiloxane hybrid membranes in desulfurization of model gasoline. Chem Eng Sci 135:479–488
Zhang SG, Zhang ZC (2002) Novel properties of ionic liquids in selective sulfur removal from fuels at room temperature. Green Chem 4:376
Zhang W, Tang J, Ye J (2007) Structural, photocatalytic, and photophysical properties of perovskite $MSnO_3$ (M = Ca, Sr, and Ba) photocatalysts. J Mater Res 22:1859
Zhao C, Li J, Qi R, Chen J, Luan Z (2008) Pervaporation separation of n heptane/sulfur species mixtures with poly dimethyl siloxane membranes. Purif Technol 63:220–225